ICAS 2021 SHANGHAI
International Council of the Aeronautical Sciences
32nd Congress of the International Council of the Aeronautical Sciences
September 6-10, 2021
Pudong Shangri-La, Shanghai, China

Adjusted shapes of adhesively bonded repair patches for the early indication of debond in fighter aircraft structures

J. Jokinen[1], M. Wallin[2], M. Kanerva[1]

[1]Tampere University, Faculty of Engineering and Natural Sciences, P.O.B 589, FI-33101 Tampere, Finland
[2]Patria Aviation, Lentokonetehtaantie 3, FI-35600 Halli, Finland

Abstract

Adhesively bonded joints are widely used in structural repairs of aeroplanes. The main disadvantages of adhesive bonding are the complex bonding process and the inability to inspect the mechanical quality of the bondline. This inability is the main limiting factor for using bonded repairs in primary structures. This work examines bonded repairs from the point of view of adjusted patch shapes. Numerical analyses are performed for studying if adjusted patch shape could provide an early indication of bondline failure and its propagation. The secondary target is to explore if damage propagation can be limited.

Keywords: bonded repair, cohesive zone model, weak bond

1. Introduction

The aeroplane's lifespan includes various flight operations that result in a fatigue spectrum and can continue to accumulate for several decades. The operations for military aeroplanes are performed in harsh operating environments. This can lead to structural damages. Adhesively bonded patches are used for structural repairs. However, the airworthiness (inspection) of the adhesive bonded repair is not straightforward. This especially refers to the complexity of the bonding process and its inspection for acceptance. Several surface preparation steps are needed for feasible adhesive bonding [1]. Of course, other manufacturing steps and mechanical design also play a major role. The bondline inspection is a valid method for studying voids in the bonded repair. However, the inspection methods are not capable of revealing surface preparation mistakes/flaws that can lead to so-called weak bonds in the structures.

The bonded repairs' inspection would be easier if an early indication could be observed in the form of local debond before the total failure of the repair. Typically, the patch shape is either circular or ellipsoidal ('racetrack'). The studies of adjusted shapes are scarce in the current literature. As a concept, the edge of the adjusted shaped in the patch would not be highly load carrying portion but it would provide the early indication of the debond initiation in the event of load limit exceedance. This could provide the possibility of visual inspection of the patch on outer surfaces. However, the adjusted shape should not increase the likelihood of the debond onset in the patch overall. Finally, for the propagation, it would be beneficial if debond is limited to an 'adequate' portion of the patch.

In this work, finite element analysis for the adjusted patch shape is studied. The studied repaired structure is a metal sheet with a small crack (through), which is covered using a metallic adhesively bonded patch. The repair and anticipated debond was analysed using the cohesive zone model (CZM). The CZM is capable of analysing debond onset and propagation. The virtual crack closure technique (VCCT) was applied also for studying the crack tip loading. We had two primary targets for our study: Firstly, we studied if the adjusted repair provides the early indication. Secondly, an interest was focused on the damage propagation in the repair overall. The target in the propagation analysis was to analyse if the debond propagation is halted before the full patch gets removed (because of the adjustment in patch shape). The analyses are performed under different loadings, patch thicknesses, and (pre) crack lengths.

2. Fracture model

The linear mixed-mode criterion for the CZM was chosen for our analysis. The criterion takes the form

$$f_{\text{damage}} = G_{\text{I}}/G_{\text{IC}} + G_{\text{II}}/G_{\text{IIC}} + G_{\text{III}}/G_{\text{IIIC}} \quad (1)$$

where G_{I}, G_{II} and G_{III} are energy release rates (ERR) provided by the numerical analysis and G_{IC}, G_{IIC} and G_{IIIC} are the critical ERR values – typically based on experimental testing. Our previous work studied the epoxy adhesive ply (FM 300-2) [2], which is a typical adhesive product in bonded repairs of aeroplanes. The critical ERR values G_{IC} and G_{IIC} in the case of FM300-2 were 1820 J/m^2 and 6230 J/m^2, respectively, and they are defined for the practical adhesive bond with acceptable cohesive failure [2]. This work has an interest to study the adjusted patch shapes when a type of adhesion (interface) failure exists in the bond. The critical ERRs are significantly higher in the event of cohesive failure mode than in the event of the interface failure. For that reason, the values were multiplied with a factor of 0.1. The mode III value was assumed to equal the mode II value. Finally, the critical ERRs used in Eq. (1) were 180 J/m^2 for mode I and 620 J/m^2 for mode II and mode III.

The CZM is modelled using a traction-separation law where the CZM zone's final failure is defined by the mixed-mode criterion (Eq. (1)). The simplest bi-linear law was used in our analysis. The law has a linear response before the damage onset, for which the cohesive stiffness was set to 10^{15} N/m^3 for all the three modes. The damage onset was defined using the quadratic stress criterion. After achieving the stress criterion's limit value, the response of the cohesive surface's stiffness will degrade in a linear manner and, finally, fail as the criterion by Eq. (1) is satisfied. The quadratic stress criterion can be extracted as

$$f_{\text{onset}} = (\sigma_{\text{I}}/\sigma_{\text{IC}})^2 + (\tau_{\text{II}}/\tau_{\text{IIC}})^2 + (\tau_{\text{III}}/\tau_{\text{IIIC}})^2 \quad (2)$$

where σ_{I}, τ_{II} and τ_{III} are evaluated by the CZM and σ_{IC}, τ_{IIC} and τ_{IIIC} are the cohesive strengths. Cohesive strengths are commonly considered as numerical parameters, for which the significance in the analysis of propagating debond is often small. The numerical approach for coarse meshes, developed by Turon et al. [3], was used for defining the cohesive strengths here. The numerical approach is based on the equation

$$\bar{\tau}^o = \sqrt{\frac{9\pi E G_{iC}}{32 N_e^o l_e}} \quad (3)$$

where E is the Young's modulus, G_{IC} is the fracture toughness (sub-index referring to the fracture mode), N_e^o is the number of elements in the cohesive zone, and l_e is the element length. We applied the adhesive's Young's modulus (of 2.45 GPa) while a separate adhesive film was not modelled. Recommendations for the number of elements in the cohesive zone range from three to ten [4]. We assumed a value of 5 and the typical element length was finally 2 mm in the structure. These assumptions provided values of 6.6 MPa (mode I) and 12.3 MPa (mode II and III).

3. Finite element model

The finite element (FE) model presenting the structure and the patch was created and analysed in Abaqus/Standard 2017 (Figure 1). Both the patch and the structure were modelled as aluminium (material model) where only linear-elastic behaviour was taken into account. Aluminium's Young's modulus was presumed 71 GPa and the Poisson's ratio of 0.3 was used in the FE models. The structure was modelled as a solid part, which had a thickness of 3.2 mm. Two types of FE models were created. The difference between these FE models was in the (symmetric) boundary conditions. Most of the analysis was performed using a quarter-model. The model for studying the crack's ERR was analysed using a half-model. The length and width of the quarter-model was 100 mm, which corresponds 200 mm and 100 mm in the half-model. The patch thickness was mainly 3.2 mm but also thickness of 1 mm (Section 4.4) was studied. The patch shape was modified during the analyses. The

reference patch was a circular one with a 50 mm-diameter. The patch was connected to the structure using the contact type based on the cohesive surface. The contact discretization was the 'surface to surface' type with 'small sliding' type of formulation.

The applied boundary conditions are shown in Figure 1. The upper edge had been subjected to enforced vertical displacement of 0.5 mm in the quarter-model and 1 mm in the half-model. The analysis was performed mainly under uniaxial loading, excluding Section 4.5. The vertical edge had the 'symmetry' type of boundary condition, which restricted the displacement in the horizontal direction. The initial crack was modelled for the quarter model using boundary conditions at the lowest edge. Two (pre) crack lengths, i.e. 2.5 mm and 10 mm, were studied in the analysis. The lowest edge's displacement was restricted in the vertical direction at the intact area. The thickness direction's displacement was restricted only at the upper edge along the symmetry boundary condition. The model was meshed using the solid (C3D8R) elements with the typical element dimension of 2 mm.

The reference and adjusted patch models were finally analysed using the VCCT. The VCCT was used for computing the ERR values at the crack tip. For the VCCT analysis, the 'vertical symmetry' type of boundary condition was removed from the lowest edge and a second plate was added below it (Figure 1). The two solid parts were connected using the VCCT's contact definition. The vertical symmetry boundary condition was changed at the bottom while still covering the whole surface. The thickness direction's displacements were limited in both upper and lower edges in the half-model.

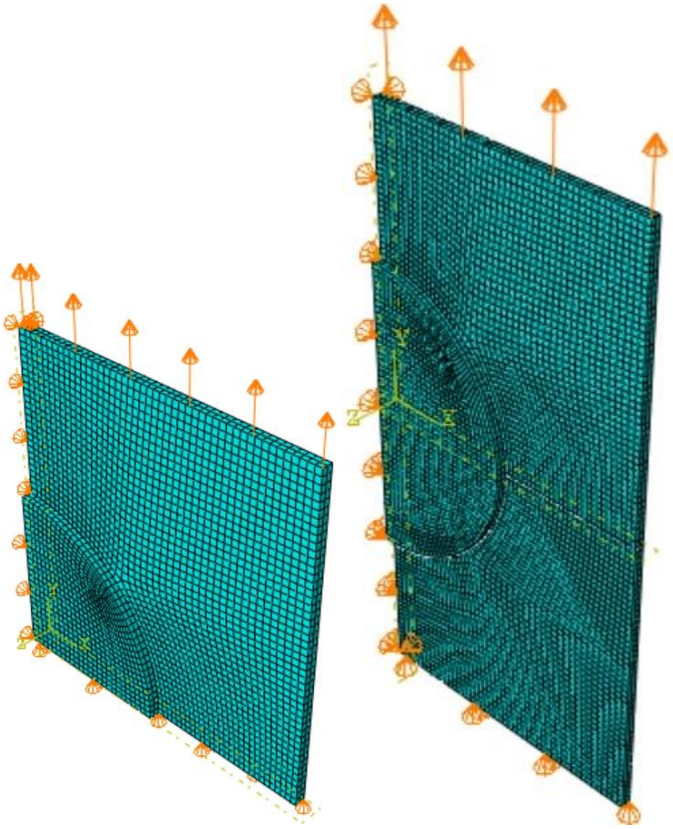

Figure 1. The quarter (left) and half (right) FE models' boundary conditions and mesh.

4. Results

4.1 The initial analysis of debond onset and propagation

The FE analysis was initiated by studying the debond onset and propagation for three patch shapes. These shapes were the reference circular patch and two geometries with an additional shape portions of 20 mm (diameter) and indicated as shape A and B. The analysis was performed by using the 2.5 mm-crack length. The results of the debond onset and propagation are shown in Figure 2 and 3 at the enforced displacement of 0.1 mm and 0.4 mm, respectively. Figures (2-3) present the CSDMG variable,

which provides the value of 1 when the mixed-mode criterion is fulfilled (fully damaged) and 0 when the quadratic stress criterion is not achieved (no damage onset). The debond onset clearly occurs at the upper edge of the patch. The changes in the patch shape transfer the location of the debond onset into the direction of the additional adjusted shape (portions). However, the debond exceeds the area of the reference circular shape for both adjusted patch shapes. The patch B's debond does not grow in a similar fashion at the lower symmetry edge than other (A). The patch A provides the worst kind of debond, which reaches the lower edge. In all the models, debond propagation is smooth in terms of deformations and no debond-arresting features were found. The patch B is better than the patch A in the sense that the debond is mostly focused on the extended shapes rather than on the reference circular patch region.

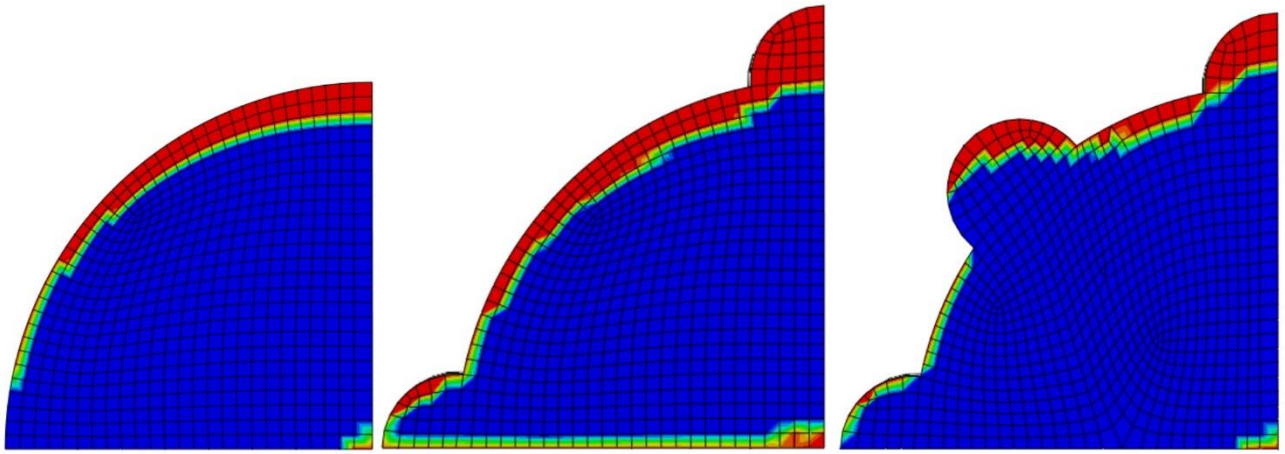

Figure 2. Patch debond for shapes: reference, A, and B, when the enforced displacement is 0.1 mm. (CSDMG / red colour is 1 (fully damaged) and blue refers to 0 (no damage))

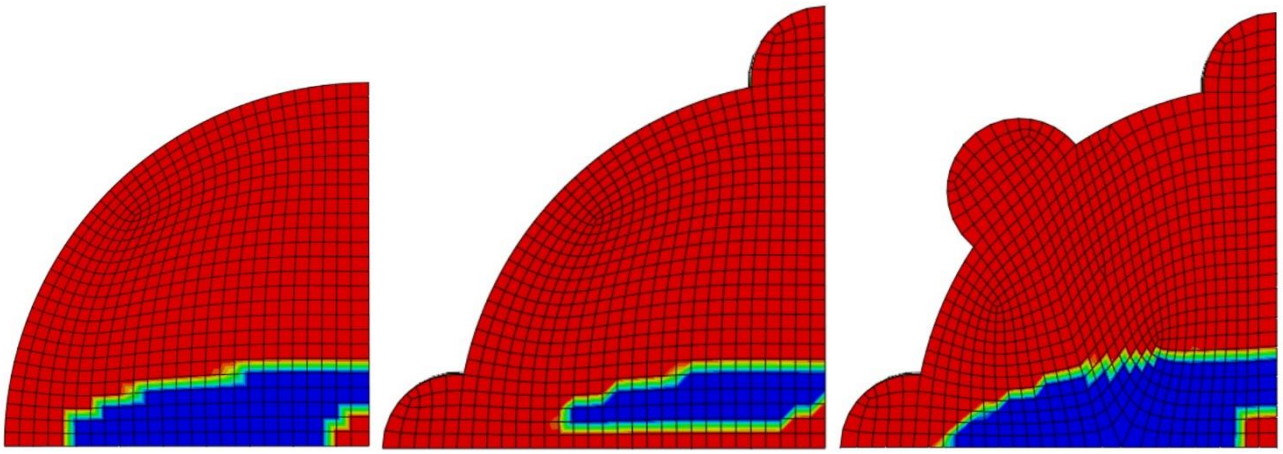

Figure 3. Patch debond for shapes: reference, A, and B, when the enforced displacement is 0.4 mm. (CSDMG / red colour is 1 (fully damaged) and blue refers to 0 (no damage))

4.2 The effects of (pre) crack length

In the next phase, the crack's length was extended (from 2.5 mm) to 10 mm. The analysis was continued running with the same three patch shapes. The patch debond surfaces are shown in Figure 4 and 5. The extension of the crack length increases the debond propagation at the lower edge of the patch but it does not significantly modify the overall debond onset and propagation behaviour.

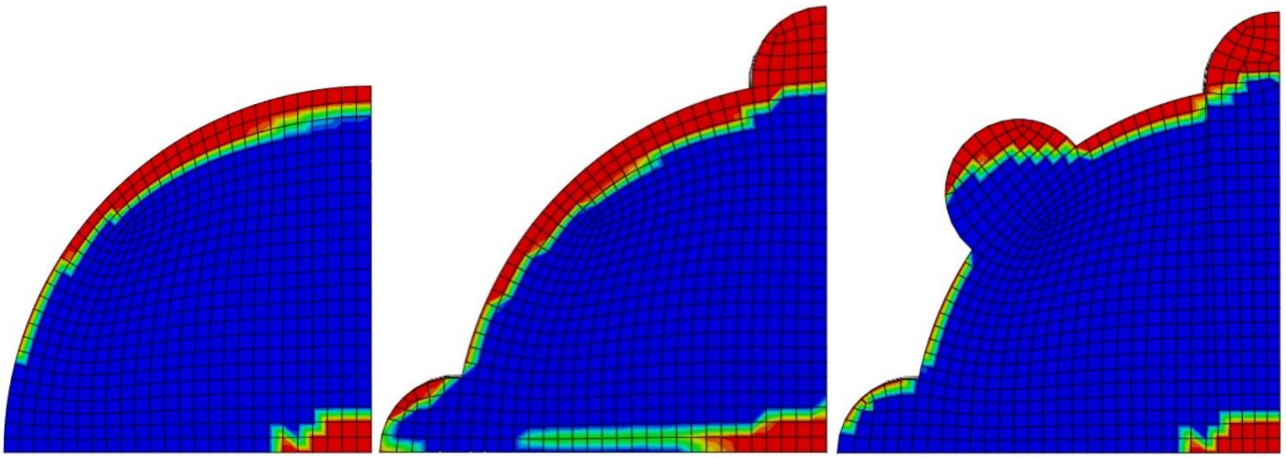

Figure 4. Patch debond for shapes: reference, A, and B, when the enforced displacement is 0.1 mm and the crack length is 10 mm. (CSDMG / red colour is 1 (fully damaged) and blue refers to 0 (no damage))

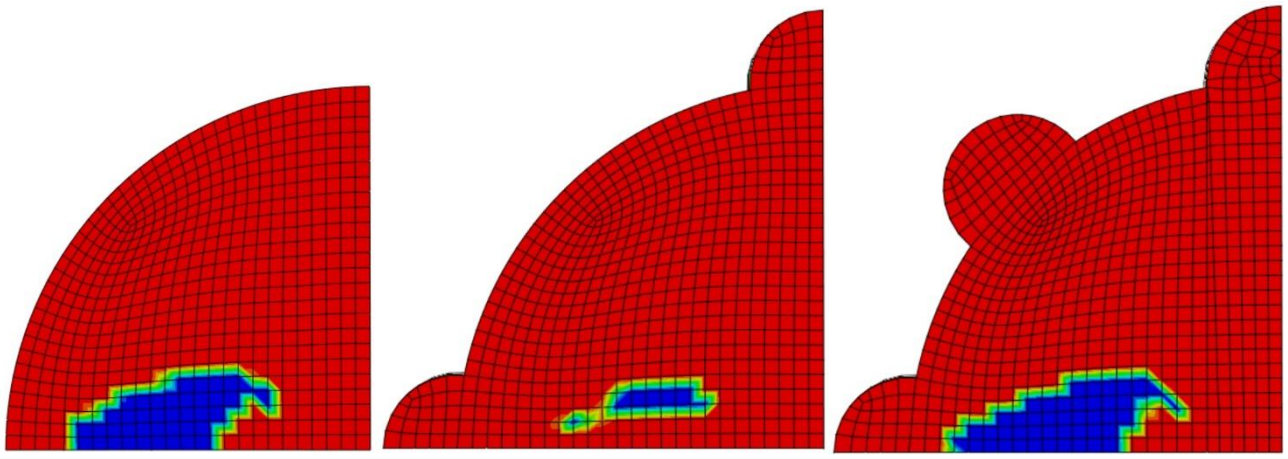

Figure 5. Patch debond for shapes: reference, A, and B, when the enforced displacement is 0.4 mm and the crack length is 10 mm. (CSDMG / red colour is 1 (fully damaged) and blue refers to 0 (no damage))

4.3 The improved patch shape

The target in general was to have the debond more focused in the adjusted portions of the patch shapes. Three new patch shapes were developed in the next phase, and the debond surfaces are shown in Figure 6 and 7. The naming convention of C, D and E is used in the following text. The circular region was modified from 50 mm to 37.5 mm in the patch C. Similar modification was made to the patch shape D but the modification in numbers was from 50 mm to 25 mm. The patch shape E had the circular region with a diameter of 37.5 mm but additionally extension portions were connected by a V-shaped connection region to the circular region (instead of diagonal and circumferential edges). Figure 6 remarks that the shapes C and D do not ‘remove’ the edge debond-type of behaviour while the propagation occurs mostly in the extension portions. The patch shape E is the most ‘feasible’ in its debond behaviour since it transfers debond into the extension portions. Figure 7 presents the fact that the patch shape D and its circular region are significantly smaller than in other patches and its debonded region is more widely spread than in the cases of patches C and E.

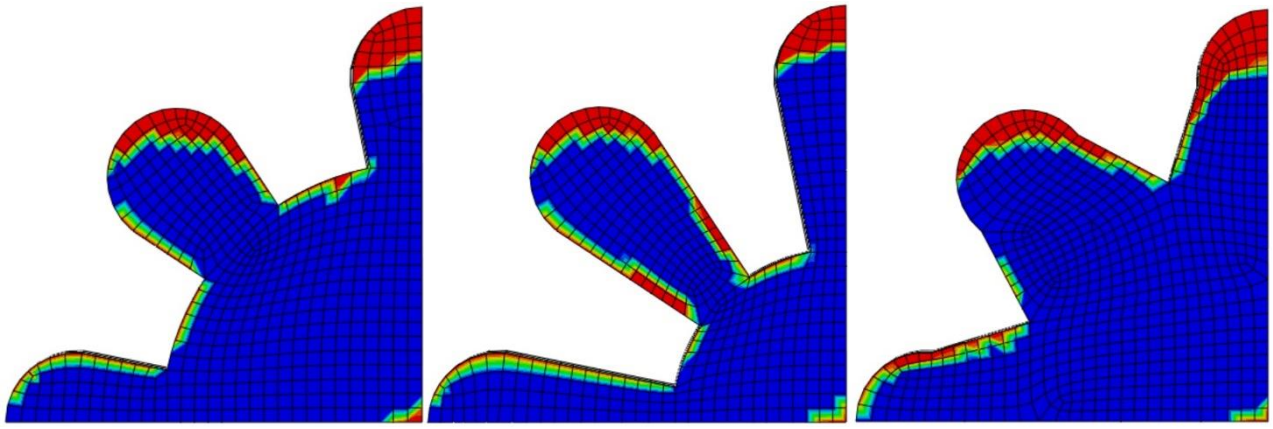

Figure 6. Patch debond for shapes: C, D, and E, when the enforced displacement is 0.1 mm. (CSDMG / red colour is 1 (fully damaged) and blue refers to 0 (no damage))

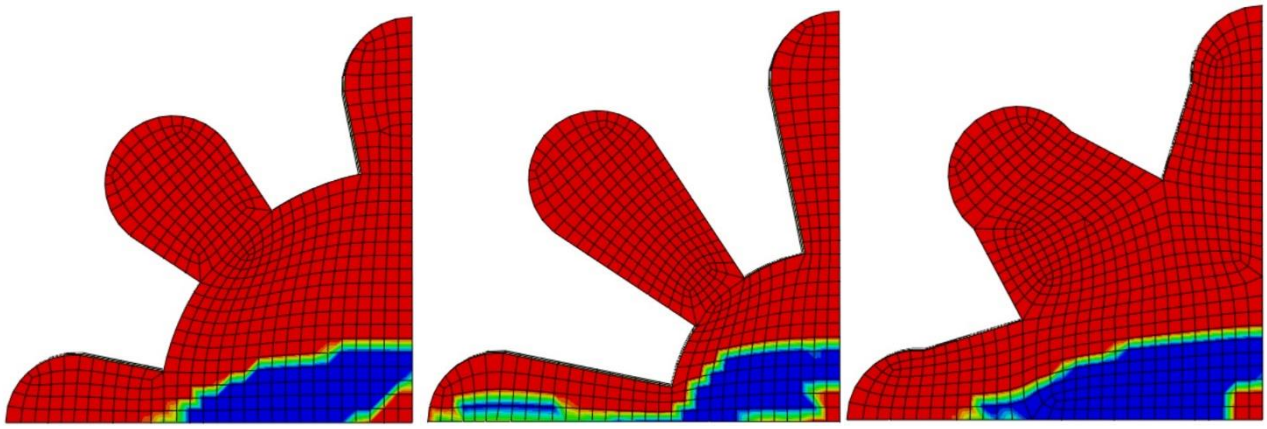

Figure 7. Patch debond for shapes: C, D, and E, when the enforced displacement is 0.4 mm. (CSDMG / red colour is 1 (fully damaged) and blue refers to 0 (no damage))

4.4 Patch thickness of 1 mm

Based on results of initial analysis, all the further analysis was focused on the reference patch and the shapes C and E. The patch thickness is typically comparable to base plate's thickness. Therefore, our initial analyses were performed with a 3.2 mm-patch thickness. The results, when the thickness is decreased from 3.2 mm to 1 mm, are shown in Figure 8 and 9. Figures show that the thinner patch leads to a smaller debonded surface area than before. The debond propagation, its direction, remains relatively similar than in the initial analyses.

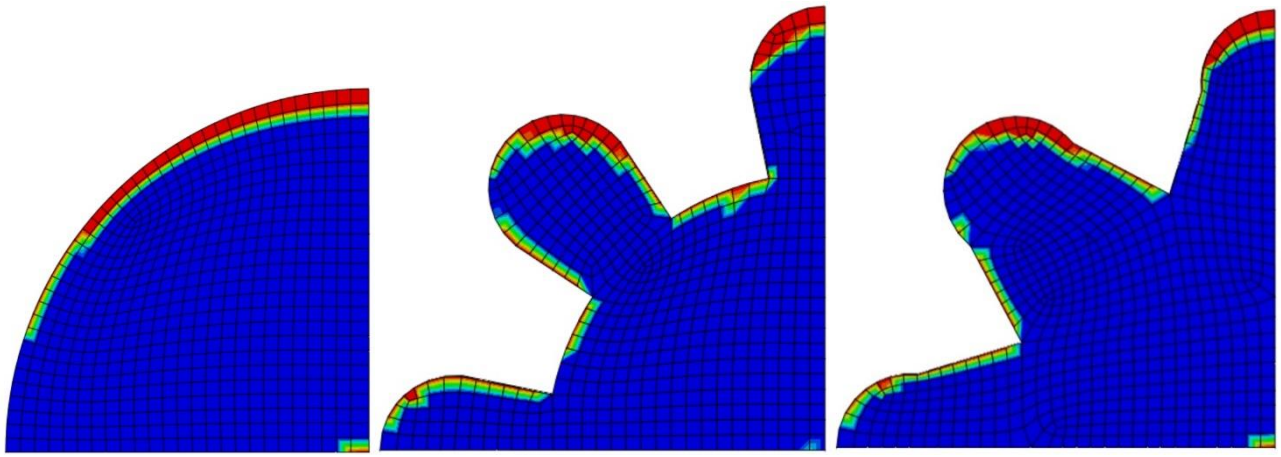

Figure 8. Patch debond for the reference, C, and E patch shapes when the enforced displacement is 0.1 mm and the patch thickness is 1 mm. (CSDMG / red colour is 1 (fully damaged) and blue refers to 0 (no damage))

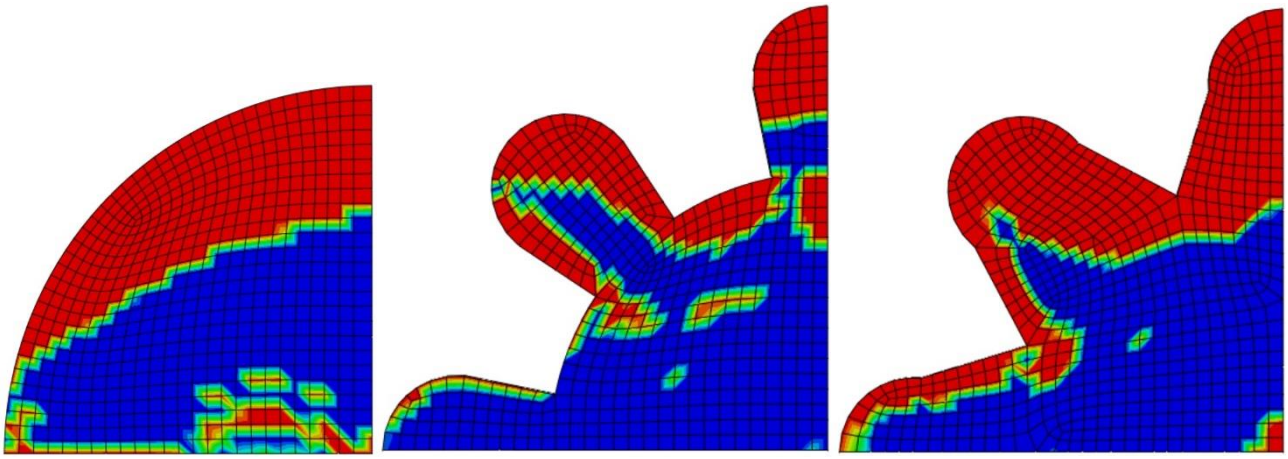

Figure 9. Patch debond for the reference, C, and E patch shapes when the enforced displacement is 0.4 mm and patch thickness is 1 mm. (CSDMG / red colour is 1 (fully damaged) and blue refers to 0 (no damage))

4.5 Bi-axial loading

Three patches (reference, shapes C and E) were analysed under bi-axial in-plane loading. The additional horizontal (in the plane of repair) loading was created using the same enforced displacement setting than for the displacement in the vertical direction. The debond surfaces under the bi-axial loading and for the three patch shapes are shown in Figure 10 and 11. The debond surface areas extend in a symmetrical manner from both (loading) directions. The patch shape E shows the most prominent behaviour from the adjusted shapes because the debond surface does not reach circular portion of the patch area with the enforced displacement of 0.1 mm. However, the patch E is also fully debonded at the enforced displacement of 0.4 mm.

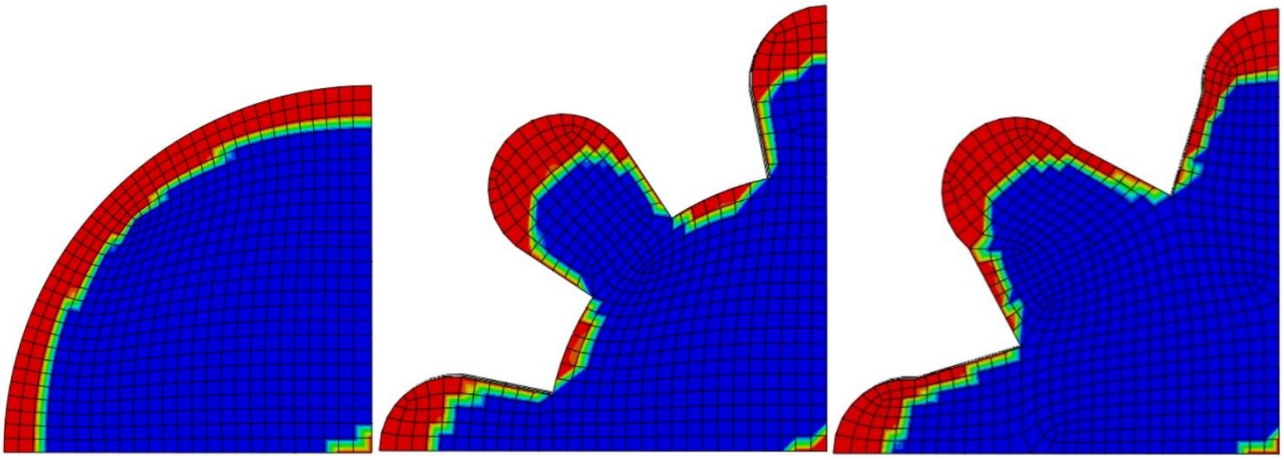

Figure 10. Patch debond for the reference, C, and E shapes when the enforced displacement is 0.1 mm in bi-axial loading. (CSDMG / red colour is 1 (fully damaged) and blue refers to 0 (no damage))

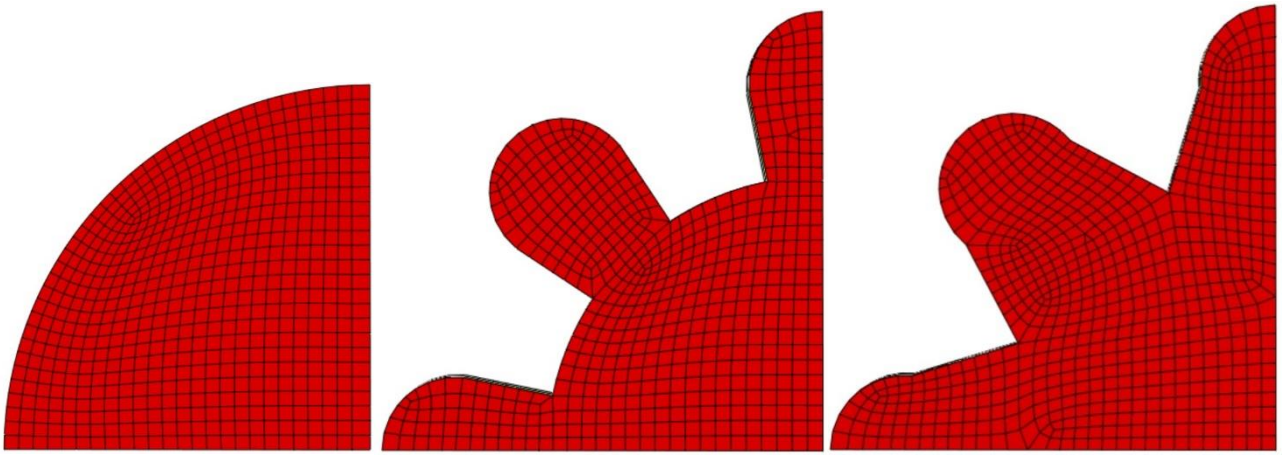

Figure 11. Patch debond for the reference, C, and E shapes when the enforced displacement is 0.4 mm in bi-axial loading. (CSDMG / red colour is 1 (fully damaged) and blue refers to 0 (no damage))

4.6 Out-of-plane deformation of the modified patches

The visual inspection of debond in a repaired structure would be a beneficial method for providing the early indication for an operator of the aeroplane. The visual inspection could be based on i.e. paint cracking caused by out-of-plane deformation at the patch edge. The out-of-plane deformation of the reference shape and the shape E for a patch was studied here. The computed out-of-plane deformations are shown in Figure 12 and 13. Figure 12 presents the deformation when the enforced displacement is 0.1 mm, which refers to the debond onset load level. The out-of-plane deformation's magnitude is less than 0.2 mm. Figure 13 presents the deformation when the enforced displacement is 0.4 mm. The shape E results in opening displacements at the patch edge. However, the range of deformation is small and hardly causing visually detectable flaw.

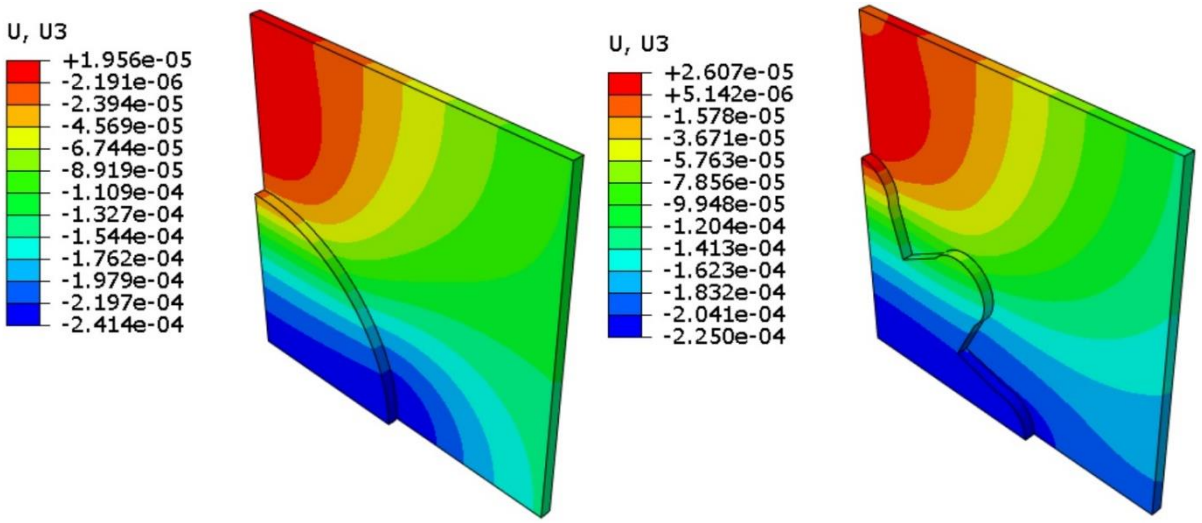

Figure 12. The out-of-plane deformation for the reference and shape E of the patch when the enforced displacement is 0.1 mm and the crack length 2.5 mm. The units of out-of-plane displacement U3 are meters.

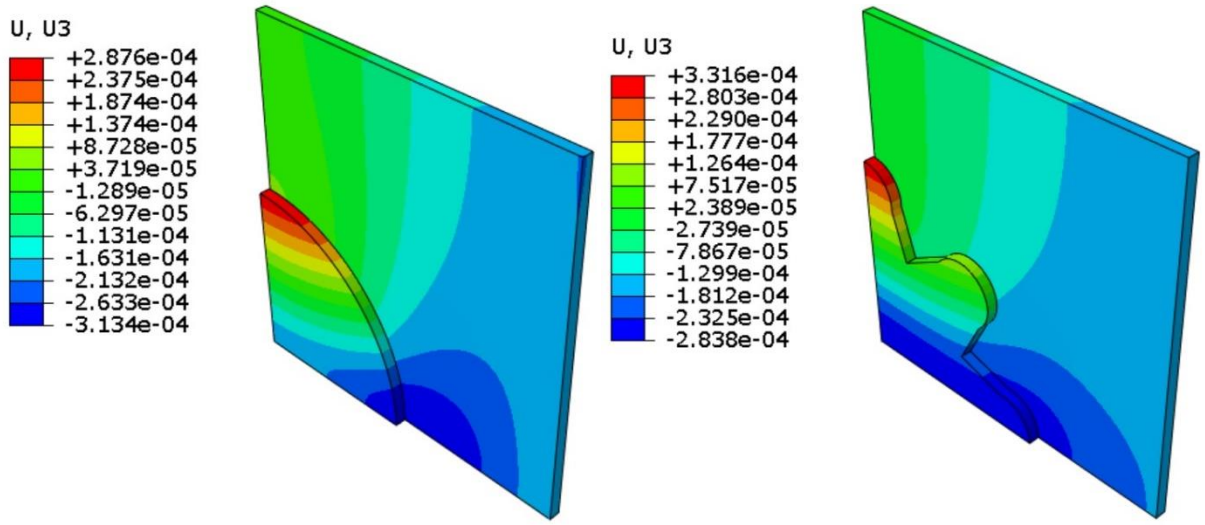

Figure 13. The out-of-plane deformation for the reference and shape E of the patch when the enforced displacement is 0.4 mm and the crack length 2.5 mm. The units of out-of-plane displacement U3 are meters.

4.7 ERR at the crack tip of debond

The target of the bonded patch repair is to reduce the loading at the original crack tip in the base structure (if not healed/drilled open). For studying the loading state, the ERR at the crack tip was analysed using the VCCT. The VCCT analyses were performed using the half-model. The half-model's length and the enforced displacement was doubled when compared to the quarter-model. The VCCT ERRs' values were taken from the nodal points at the crack tip. The fracture modes II and III and their ERR values were meaningless and the focus was subjected to the mode I ERR. ERRs for the reference and the shape C and E modifications are shown in Figure 14. The crack tip's nodal point providing the highest ERR value is located at the opposite surface (to the patch). The patch shape's adjustment is shown to decrease ERR values in both locations (patch side, bottom of base plate).

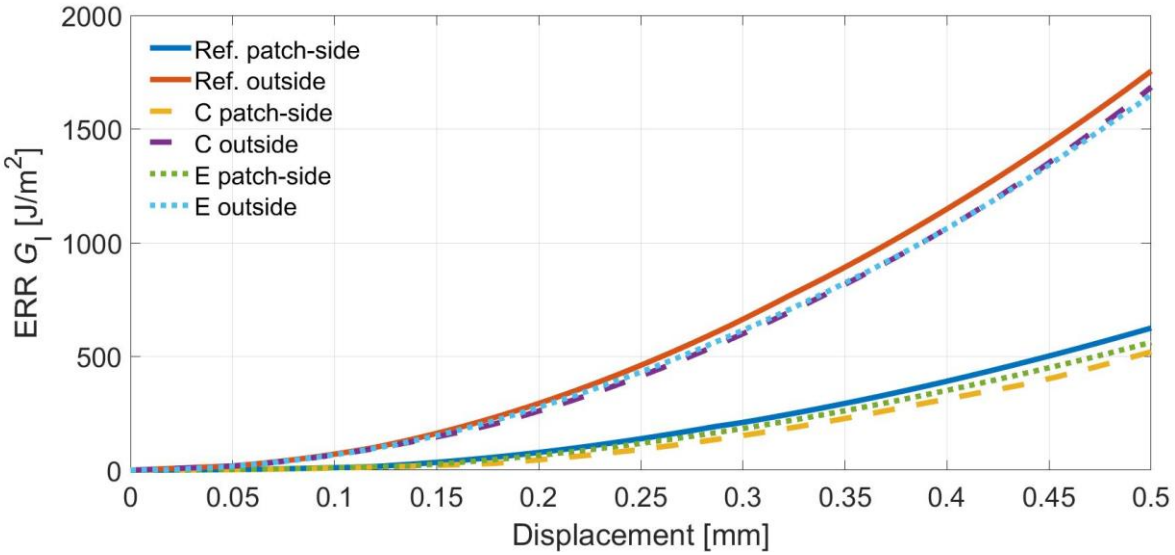

Figure 14. The crack tip's ERR value as a function of the half-model's displacement.

5. Discussion and conclusion

This work studied the applicability of the so-called adjusted shapes of repair patches for the adhesively bonded repair. Based on the analysis, the debond onset occurred essentially at the same load level in the modified patch repairs than in the circular reference patch. The likelihood of failure was not increased, however, it was not decreased either. The location of the debond onset was relatively similar to the reference shape while the adjustments in the shape transferred the onset location more towards the adjusted portion of the patch.

The currently analysed adjusted shapes were not able to limit or halt debond propagation. The debond onset and propagation, their behaviour, were not significantly altered when analysing a larger (pre) crack or thinner patch thickness. The applied adjusted shapes and dimensions did not lead to clear visual indication in terms of out-of-plane deformation – which would be beneficial for the early indication of debond onset. The studied adjusted shapes were noticed to decrease the ERR values at the crack tip when compared to the reference patch shape. This could be partly explained by difference in the reaction force when the enforced displacement was used in analysis.

Based on our study, the adjusted shapes were not noticed to significantly improve the potential to early indication or limit or slow down the debond propagation. For the future work, different adjusted shapes should be studied. Future work should also cover other effects than debond propagation. These include patch stress concentrations and fatigue. Future studies should also be performed under different loading conditions. It is important to note that constant critical ERR was presumed in the simulations here. In reality, debond onset is typically due to degraded adhesion (lower ERR) locally.

6. Acknowledgements

Authors want to acknowledge Ari Kivistö (Finnish Defence Force Logistics Command) for providing industrial reference, inspiration and motivation for the study.

7. Contact Author Email Address

mailto: jarno.jokinen@tuni.fi

8. Copyright Statement

References

[1] Aakkula J, Jokinen J, Saarela O, Tervakangas S, Testing and modelling of DIARC plasma coated elastic-plastic steel wedge specimens, *International Journal of Adhesion and Adhesives*, Vol. 68, pp. 219-228, 2016. http://dx.doi.org/10.1016/j.ijadhadh.2016.03.024

[2] Jokinen J, Orell O, Wallin M, Kanerva M. A concept for defining mixed-mode behaviour of tough epoxy film adhesives by single specimen design, *Journal of Adhesion Science and Technology*, Vol. 34, pp. 1982-1999, 2020. https://doi.org/10.1080/01694243.2020.1746606

[3] Turon A, Dávila C, Camanho P, Costa J. An engineering solution for mesh size effects in the simulation of delamination using cohesive zone models. *Engineering Fracture Mechanics*, Vol. 74, pp. 1665–82, 2007. https://doi.org/10.1016/j.engfracmech.2006.08.025

[4] Turon A. Simulation of delamination in composites under quasi-static and fatigue loading using cohesive zone models, *PhD thesis*, Universitat de Girona, 2006